PRAMANA — journal of physics

Vol. 80, No. 6
June 2013
pp. 953–970

Microscopic study of positive-parity yrast bands of $^{224-234}$Th isotopes

DAYA RAM, RANI DEVI* and S K KHOSA

Department of Physics and Electronics, University of Jammu, Jammu 180 006, India
*Corresponding author. E-mail: rani_rakwal@yahoo.co.in

MS received 16 November 2012; revised 8 February 2013; accepted 18 March 2013

Abstract. The positive-parity bands in $^{224-234}$Th are studied using the projected shell model (PSM) approach. The energy levels, deformation systematics, $B(E2)$ transition probabilities and nuclear g-factors are calculated and compared with the experimental data. The calculation reproduces the observed positive-parity yrast bands and $B(E2)$ transition probabilities. Measurement of $B(E2)$ transition probabilities for higher spins and g-factors would be a stringent test for our predictions. The results of theoretical calculations indicate that the deformation systematics in $^{224-234}$Th isotopes depend on the occupation of low k components of high j orbits in the valence space and the deformation producing tendency of the neutron–proton interaction operating between spin orbit partner (SOP) orbits, the $[(2g_{9/2})_\pi–(2g_{7/2})_\nu]$ and $[(1i_{13/2})_\pi–(1i_{11/2})_\nu]$ SOP orbits in the present context. In addition, the deformation systematics also depend on the polarization of $(1h_{11/2})_\pi$ orbit. The low-lying states of yrast spectra are found to arise from 0-quasiparticle (qp) intrinsic states whereas the high-spin states turn out to possess composite structure.

Keywords. Projected shell model; yrast energies; band diagram; electromagnetic quantities.

PACS Nos 21.60.Cs; 21.10.Ky; 21.10.Re

1. Introduction

The study of decay schemes arising from fusion evaporation reactions has greatly enhanced our understanding of nuclear structure. The spectroscopy of heavy elements has become possible with the advent of third-generation GAMMASPHERE [1] detector arrays. Thorium is one of the isotopic mass chains that has been studied. The level schemes of some of the even–even isotopes of thorium have been extended up to spin 30^+. Besides this, the experimental data are now available for electromagnetic properties also [2–11]. The level schemes of $^{224-234}$Th isotopes are characterized by the existence of two bands of opposite parity. Azmal *et al* [4] and Cocks *et al* [11] have studied the spectroscopy of $^{226-234}$Th isotopes using multinucleon transfer reactions. The positive-parity bands in $^{224-234}$Th are now extended up to spins 18^+, 20^+, 22^+, 24^+, 30^+ and 24^+. Hausser *et al* [10] measured the g-factors of high-spin states in ^{232}Th and found that the g-factors increase above spin $18\hbar$. The increase of g-factors above spin $18\hbar$ is the first direct evidence for rotational alignment of $1i_{13/2}$ protons in ^{232}Th. The experimental g-factors of states with $I \leq 16\hbar$ are lower than those for higher spins, giving experimental evidence for the alignment of $1j_{15/2}$ neutrons in ^{232}Th.

Even–even thorium nuclei have been studied within the framework of the spdf interacting boson model [12] and the results indicate that the properties of the low-lying states can be understood without the stable octupole deformation. High spin states in some of these nuclei suggest that octupole deformations develop at higher spins. Diab [13] investigated the low-lying collective levels in $^{224-234}$Th in the framework of the interacting boson approximation (IBA-1) and successfully reproduced the ground state and other bands. Diebel and Mosel [14] have studied ^{232}Th in the framework of cranked Hartree–Fock–Bogoliubov (CHFB) and calculated the neutron and proton alignments. The calculated neutron alignment for ^{232}Th was in agreement with experimental data but the proton alignment showed discrepancy. Nazarewicz and Olanders [15] have studied the rotational spectrum of some thorium nuclei using Woods–Saxon–Bogoliubov cranking method and discussed the influence of octupole deformation on high-spin properties of nuclear spectra. Egido and Ring [16] have carried out cranking model and rotating shell model (RSM) calculations to investigate the high-spin behaviour of yrast line in ^{230,232}Th. They found that a self-consistent calculation is only meaningful if it includes the number projection as well as quadrupole pairing. The RSM calculations reproduce well the alignment and band-crossing at the yrast line in these nuclei.

The purpose of the present work is to interpret the even–even positive-parity yrast bands of $^{224-234}$Th in the framework of projected shell model (PSM). In the present study, the results are obtained for positive-parity yrast bands, BCS occupation numbers, band diagrams, g-factors and $B(E2)$ transition probabilities of the $^{224-234}$Th isotopes. The calculations are carried out by including quadrupole and monopole pairing effects. The PSM results give an indication that occupation of low k-components of high j orbits in the valence space and np-interaction in SOP orbits plays a crucial role in determining the overall deformation systematics of $^{224-234}$Th isotopes. The results on band diagrams show that the yrast spectra of lower spin states in Th isotopes arise from a single 0-qp intrinsic state. As one goes to higher angular momentum states, it is observed that the intrinsic state changes and has multi-quasiparticle configuration. Some of the angular momentum states are found to have composite structure, that is, they arise from more than one intrinsic states. The observed dip in the $B(E2)$ values of ^{232}Th at $I = 22^+$ is also reproduced by the present PSM calculations. The present calculation however does not reproduce the relative positioning of the negative-parity bands with respect to the corresponding ground states of positive-parity bands.

The paper is organized as follows: In §2, an outline of PSM approach is presented. In §3, a systematic description of the deformation systematics and comparison of the calculated and observed positive-parity bands of $^{224-234}$Th isotopes are presented. Besides this, in order to check the reliability of the PSM wave function, the $B(E2)$ transition probabilities and g-factors are also compared with the experimental data. Finally, in §4, various conclusions drawn from the present analysis are presented.

2. Calculational framework

The projected shell model (PSM) is a very often used and successful method for studying medium and heavy deformed nuclei [17–22]. The detailed description of PSM can be found in [17]. The wave function in the PSM is given by

$$|\sigma, \mathrm{IM}\rangle = \sum_{K,\kappa} f_\kappa^\sigma \hat{P}^I_{M\,K}\, |\phi_\kappa\rangle. \tag{1}$$

The index σ denotes the states with the same angular momentum and κ the basis states. $\hat{P}^I_{M\,K}$ is the angular momentum projection operator and f_κ^σ are the weights of the basis states κ.

We have assumed axial symmetry for the basis states and the intrinsic states are, therefore, the eigenstates of the K-quantum number. For calculating an even–even system, the following four kinds of basis states $|\phi_\kappa\rangle$ are considered: the quasiparticle (qp) vacuum $|0\rangle$, two-quasineutron states $a^\dagger_{\nu_1} a^\dagger_{\nu_2}\,|0\rangle$, two-quasiproton states $a^\dagger_{\pi_1} a^\dagger_{\pi_2}\,|0\rangle$ and two-quasineutron plus two-quasiproton (or 4-qp) states $a^\dagger_{\nu_1} a^\dagger_{\nu_2} a^\dagger_{\pi_1} a^\dagger_{\pi_2}\,|0\rangle$. The projected vacuum $|0\rangle$, for instance, is the ground-state band (g-band) of an even–even nucleus. The weight factors f_κ^σ in eq. (1) are determined by diagonalization of the shell model Hamiltonian in the space spanned by the projected basis states given above. This leads to the eigenvalue equation

$$\sum_{\kappa'} (H_{\kappa\,\kappa'} - E_\sigma N_{\kappa\,\kappa'}) f^\sigma_{\kappa'} = 0 \tag{2}$$

and the normalization is chosen such that

$$\sum_{\kappa\kappa'} f_\kappa^\sigma N_{\kappa\kappa'} f^{\sigma'}_{\kappa'} = \delta_{\sigma\sigma'}, \tag{3}$$

where the Hamiltonian and norm-matrix elements are given by

$$H_{\kappa\kappa'} = \langle\phi_\kappa|\hat{H}\,\hat{P}^I_{K_\kappa K'_{\kappa'}}|\phi_{\kappa'}\rangle \tag{4}$$

$$N_{\kappa\kappa'} = \langle\phi_\kappa|\hat{P}^I_{K_\kappa K'_{\kappa'}}|\phi_{\kappa'}\rangle. \tag{5}$$

In the numerical calculations, we have used the standard quadrupole–quadrupole plus (monopole and quadrupole) pairing force, i.e.,

$$H = \hat{H}_0 - \frac{1}{2}\chi \sum_\mu \hat{Q}^\dagger_\mu \hat{Q}_\mu - G_M \hat{P}^\dagger \hat{P} - G_Q \sum_\mu \hat{P}^\dagger_\mu \hat{P}_\mu. \tag{6}$$

This separable-force Hamiltonian [17] has been used successfully to explain the system of rotational spectra for a large number of nuclei. In eq. (6), $\hat{H}_0$ is the spherical single-particle Hamiltonian, which contains a proper spin-orbit force [23]. The remaining terms in the equation are residual quadrupole–quadrupole, monopole pairing and quadrupole pairing interactions, respectively. The strength χ of the quadrupole–quadrupole term can be obtained via self-consistent mean-field HFB calculation with a given deformation parameter ε_2.

Table 1. Quadrupole and hexadecapole deformation parameters used in the present calculations.

Th	224	226	228	230	232	234
ε_2	0.220	0.230	0.240	0.244	0.250	0.250
ε_4	−0.050	−0.040	−0.040	−0.050	−0.050	−0.050

The strength of the quadrupole force χ is adjusted such that the known quadrupole deformation parameter ε_2 is obtained. The monopole pairing strength G_{M} is of the form

$$G_{\mathrm{M}} = \left(G_1 \mp G_2 \frac{N-Z}{A}\right) \frac{1}{A} (\mathrm{MeV}) \tag{7}$$

with $-$ for neutrons and $+$ for protons. Here, G_1 and G_2 are taken as 20.12 and 13.13, respectively. The strength of the quadrupole–quadrupole pairing force, G_{Q}, is assumed to be proportional to G_{M}. One may carefully adjust the ratio of $G_{\mathrm{Q}}/G_{\mathrm{M}}$ during the calculation to get the best representation of experimental observation. In the present calculation, the ratio $G_{\mathrm{Q}}/G_{\mathrm{M}}$ is fixed as 0.24 for $^{224-226}$Th, 0.22 for ^{228,230}Th and 0.16 for ^{232,234}Th. In our calculations we have taken three major shells $N = 4, 5, 6$ (5, 6, 7) for protons (neutrons) for the valence single-particle space, i.e., the inert core is taken as $Z = 40$ and $N = 70$. The multi-quasiparticle basis selection is carried out from $N = 6$ intruder shell for protons and $N = 7$ for neutrons. The deformed Nilsson single-particle (SP) states are generated with the deformation parameters listed in table 1. The values of quadrupole deformation parameters are nearly the same as adopted by Raman *et al* [8,9]. The multiparticle configurations are constructed from the Nilsson single-particle states near the Fermi levels.

In short, the procedure of the present calculation is that, based on a deformed Nilsson potential with pairing included in the BCS treatment, one performs explicit angular momentum projection with a two-body interaction which conforms (through self-consistent conditions) with the mean-field Nilsson potential. The Hamiltonian with separable forces serves as an effective interaction, the strengths of which have been fitted to experimental data. The deformed single-particle states with deformation parameters ε_2 are used solely as a starting basis. It is sufficient for the calculation to have these deformation parameters close to the observed nuclear deformation. After diagonalizing the Hamiltonian in the quasiparticle basis, the lowest energy for each spin is used to compare with the experimental yrast energy. The resulting wave functions are usually used to compute the $E2$ transition strengths and gyromagnetic (g-) factors [24].

3. Results and discussion

3.1 *Deformation trends in thorium isotopes*

In table 2, the results of E_2^+, E_4^+ and E_4^+/E_2^+, both experimental and theoretical, are presented. From the systematics of the observed 2^+ states, one notes that there is a slow

Table 2. Comparison of experimental (Exp.) and calculated (Th.) excitation energies (in units of MeV) of 2_1^+ $\left(E_2^+\right)$, 4_1^+ $\left(E_4^+\right)$ and E_4^+/E_2^+ ratio.

	Exp.			Th.		
Nucleus	E_2^+	E_4^+	E_4^+/E_2^+	E_2^+	E_4^+	E_4^+/E_2^+
^{224}Th	0.098	0.284	2.898	0.0875	0.2861	3.267
^{226}Th	0.072	0.226	3.139	0.0704	0.2319	3.294
^{228}Th	0.057	0.186	3.263	0.0576	0.1905	3.307
^{230}Th	0.053	0.174	3.283	0.0544	0.1801	3.310
^{232}Th	0.049	0.162	3.306	0.0503	0.1668	3.316
^{234}Th	0.049	0.163	3.326	0.0490	0.1629	3.324

decrease in the value of this quantity as one moves from ^{224}Th to ^{232}Th. In ^{224}Th, the value of E_2^+ is 0.098 MeV whereas in ^{232}Th its value is 0.049 MeV. Thereafter, the value of E_2^+ energy remains constant. Similar trend is exhibited by E_4^+ values. The value of E_4^+ for ^{224}Th is 0.284 MeV and its value for ^{234}Th is 0.163 MeV. From the study of literature, it is known through Grodzins relation that E_2^+ energy is inversely related to the quadrupole deformation in the nucleus. According to Grodzins rule [25], a decrease in E_2^+ energy manifests itself in the increase of quadrupole deformation. Therefore, from the observed systematics of the 2^+ states one infers that there is an increase of quadrupole collectivity in the Th isotopic mass chain as one proceeds from ^{224}Th to ^{234}Th. The observed trend of the increase of deformation in going from $^{224-234}$Th is also confirmed by the systematics of the observed $B(E2;\, 2 \rightarrow 0)$ values. It has been cited in [26] that ratio of E_4^+/E_2^+ energies is a good parameter for assessing the shape deformation of a nucleus. For a vibrational type of nucleus, the value of this ratio is around 2 whereas its value for rigid rotator is around 3.33. Thus, a value between 2 and 3.33 indicates that the nucleus is quasideformed. From the systematics of E_4^+/E_2^+ values, one notices that this ratio systematically increases as one moves from ^{224}Th to ^{234}Th. Its value for ^{224}Th is 2.898 whereas its value for ^{234}Th is 3.326. This ratio also gives evidence of the gradual build-up of deformation in Th isotopic mass chain as one moves from ^{224}Th to ^{234}Th. In the same table, the theoretical values for E_2^+, E_4^+ and E_4^+/E_2^+ are also presented. It is noteworthy that the calculated E_2^+ systematics are very close to the observed E_2^+ systematics. Besides, the systematics of the calculated E_4^+ values follow nearly the same trend as the observed ones. Their values are also very close to the observed values. Similar trend is also shown by the calculated ratios of E_4^+/E_2^+ values. It is known from the laws of microscopic physics that the systematics of E_2^+, E_4^+ and E_4^+/E_2^+ observed in $^{224-234}$Th isotopes depend crucially on the intrinsic nature of the wave function as it is well known from quantum physics that all properties are obtained from the wave function. Thus, in order to understand the observed systematics of low-lying states in Th isotopes, it is important to study the intrinsic wave function for protons and neutrons.

In tables 3 and 4, the results of BCS occupation probabilities for protons and neutrons of the valence orbits for the Th isotopic mass chain are presented. Before discussing

Table 3. The BCS subshell occupation numbers of protons in the ground state of $^{224-234}$Th isotopes.

Nucleus	^{224}Th	^{226}Th	^{228}Th	^{230}Th	^{232}Th	^{234}Th
$3s_{1/2}$	1.72	1.67	1.62	1.61	1.61	1.61
$2d_{3/2}$	3.61	3.54	3.48	3.47	3.47	3.47
$2d_{5/2}$	5.87	5.84	5.83	5.83	5.83	5.83
$1g_{7/2}$	7.90	7.88	7.87	7.88	7.88	7.88
$1g_{9/2}$	9.96	9.96	9.96	9.96	9.96	9.96
$3p_{1/2}$	0.12	0.12	0.13	0.14	0.14	0.14
$3p_{3/2}$	0.40	0.43	0.46	0.47	0.47	0.47
$2f_{5/2}$	0.57	0.60	0.63	0.64	0.64	0.64
$2f_{7/2}$	1.52	1.57	1.60	1.59	1.59	1.59
$1h_{9/2}$	3.17	3.25	3.27	3.22	3.23	3.23
$1h_{11/2}$	11.16	11.03	10.91	10.90	10.89	10.88
$4s_{1/2}$	0.005	0.005	0.006	0.006	0.006	0.006
$3d_{3/2}$	0.007	0.008	0.008	0.009	0.009	0.009
$3d_{5/2}$	0.04	0.04	0.05	0.06	0.06	0.06
$2g_{7/2}$	0.02	0.02	0.03	0.03	0.03	0.03
$2g_{9/2}$	0.36	0.38	0.41	0.44	0.44	0.44
$1i_{11/2}$	0.09	0.09	0.10	0.10	0.10	0.10
$1i_{13/2}$	3.46	3.54	3.63	3.64	3.63	3.62

the results of occupation probabilities, it is necessary to discuss and highlight some of the accepted factors responsible for bringing in sizeable collectivity in the nuclei. It is generally felt that the neutron–proton (n–p) effective interactions possess a deformation-producing tendency and the neutron–neutron (n–n) or proton–proton (p–p) effective interactions are mostly of the pairing nature [27–32]. These ideas have played pivotal roles in the development of the stretch scheme of Danos and Gillet [30], rotor model of Arima and Gillet [31] and the interacting boson model of Arima *et al* [32]. In this regard, the role of n–p interaction in SOP orbits in the context of the general development of collective features was suggested by Federman and Pittel [27,33–35] and also by Casten *et al* [26]. Their calculation provided evidence suggesting that n–p interaction between the valence nucleons in the SOP orbits, the orbits $(1g_{9/2})_\pi$ and $(1g_{7/2})_\nu$, in the zirconium and molybdenum nuclei may be instrumental *vis-à-vis* the observed onset of deformation in Mo isotopes with $A > 100$. It may also be pointed out that the role of n–p interaction operating between SOP orbits in producing deformation depends critically on the relative occupation probability of $(1g_{9/2})_\pi$ and $(1g_{7/2})_\nu$ orbits [36]. In addition to this factor, the collectivity in a nucleus can also result due to the occupation of low k-components of a high j orbit in the valence space. Besides this, polarization of an inert core can also bring in quadrupole collectivity in a nucleus as a completely full shell is known to possess zero quadrupole moment. In the light of these factors, an attempt now will be made to explain the observed systematics of low-lying states in $^{224-234}$Th.

Table 4. The BCS subshell occupation numbers of neutrons in the ground state of $^{224-234}$Th isotopes.

Nucleus	^{224}Th	^{226}Th	^{228}Th	^{230}Th	^{232}Th	^{234}Th
$3p_{1/2}$	1.08	1.18	1.30	1.57	1.88	1.95
$3p_{3/2}$	3.50	3.57	3.66	3.81	3.94	3.96
$2f_{5/2}$	5.21	5.33	5.48	5.72	5.91	5.95
$2f_{7/2}$	7.90	7.90	7.93	7.96	7.98	7.98
$1h_{9/2}$	9.88	9.89	9.92	9.95	9.98	9.98
$1h_{11/2}$	11.97	11.98	11.98	11.99	11.99	11.99
$4s_{1/2}$	0.17	0.17	0.19	0.20	0.21	0.28
$3d_{3/2}$	0.27	0.29	0.32	0.34	0.37	0.57
$3d_{5/2}$	0.89	0.99	1.08	1.10	1.13	1.17
$2g_{7/2}$	0.94	1.03	1.12	1.16	1.22	1.33
$2g_{9/2}$	2.46	3.80	3.02	3.11	3.29	3.73
$1i_{11/2}$	2.93	3.34	3.72	3.98	4.38	4.76
$1i_{13/2}$	12.65	11.74	12.90	13.26	13.56	13.65
$4p_{1/2}$	0.003	0.003	0.003	0.004	0.003	0.004
$4p_{3/2}$	0.008	0.010	0.011	0.010	0.009	0.03
$3f_{5/2}$	0.08	0.13	0.18	0.22	0.26	0.26
$3f_{7/2}$	0.06	0.12	0.14	0.14	0.16	0.53
$2h_{9/2}$	1.18	1.36	1.54	1.69	1.78	1.95
$2h_{11/2}$	0.36	0.40	0.44	0.45	0.48	0.84
$1j_{13/2}$	1.82	1.87	1.92	1.91	1.94	1.95
$1j_{15/2}$	3.06	3.26	2.26	3.52	3.55	3.57

The subshell occupation numbers presented in tables 3 and 4 have been calculated from the zero quasiparticle intrinsic wave function generated for $^{224-234}$Th isotopes. A study of the band diagrams for $^{224-234}$Th reveals that energy states with spin $\leq 16\hbar$ are obtained from the zero quasiparticle intrinsic wave function. Therefore, careful examination of occupation probabilities reveals the following:

(i) It is observed from table 3 that the proton orbits $2d_{3/2}$, $2d_{5/2}$, $1g_{7/2}$ and $1g_{9/2}$ are meagerly polarized and their occupation remains almost constant as one moves from ^{224}Th to ^{234}Th. The occupation of these orbits does not play any role in the development of quadrupole collectivity as one proceeds from ^{224}Th to ^{234}Th.

(ii) From the same results presented in table 3, it is observed that the down-slopping $k = 1/2$ components of $2f_{5/2}$, $2f_{7/2}$ and $2g_{9/2}$ orbits are getting occupied with their occupation number systematically increasing as one goes from ^{224}Th to ^{234}Th. Besides this, it is observed that $k = 1/2, 3/2$ components of $1h_{9/2}$ and $1i_{13/2}$ proton orbits are getting occupied with their occupations increasing from 3.17 and 3.46 in ^{224}Th to 3.23 and 3.62 in ^{234}Th respectively producing an increase in deformation in synergy with the earlier effect as one proceeds from ^{224}Th to ^{234}Th.

(iii) From the same table, it is observed that the $(1h_{11/2})_\pi$ orbit gets increasingly polarized as one proceeds from ^{224}Th to ^{234}Th. In ^{224}Th, the occupation of $(1h_{11/2})_\pi$

is 11.16 whereas its occupation in ^{234}Th is 10.88. This increased polarization of $(1h_{11/2})_\pi$ orbit is responsible for the increase in collectivity.

(iv) From table 4, it is observed that the neutron occupation probabilities of $2g_{7/2}$, $2g_{9/2}$, $1i_{11/2}$, $2h_{9/2}$ and $1j_{15/2}$ orbits systematically increase towards the midshell values with increasing neutron number, resulting in a systematic increase in the deformation in Th isotopes.

(v) The $2g_{9/2}$ proton occupation is found to suffer a slow increase from its value of 0.36 for ^{224}Th to 0.44 for ^{234}Th. The occupation probability of $2g_{7/2}$ neutron subshell is also found to increase from 0.94 to 1.35 as one moves from ^{224}Th to ^{234}Th. This therefore, produces an opportunity for the n–p interaction between the SOP orbits $[(2g_{9/2})_\pi\text{–}(2g_{7/2})_\nu]$ to operate and produce deformation in the nucleus. The effectiveness to do so increases with increase in the occupation of $2g_{7/2}$ neutron orbit. Note that $2g_{7/2}$ neutron occupation systematically increases from ^{224}Th to ^{234}Th, thus contributing for producing the desired systematics of low-lying states in Th isotopic mass chain. This effect is strengthened because of the largeness of the two-body effective interaction matrix elements between SOP orbits.

(vi) The occupation probabilities of $1i_{13/2}$ proton orbit are found to slightly increase from 3.46 in ^{224}Th to 3.62 in ^{234}Th and the occupation probability of $1i_{11/2}$ neutron subshell increases from 2.93 in ^{224}Th to 4.76 in ^{234}Th. This pattern of occupation numbers for this pair of SOP orbits $[(1i_{13/2})_\pi\text{–}(1i_{11/2})_\nu]$ can effectively result in the increase of deformation as one moves from ^{224}Th to ^{234}Th.

Thus, the observed systematics of low-lying states in ^{224}Th to ^{234}Th and the deformation trend observed in these isotopes could intricately be linked to the pattern of occupation probabilities of valence orbits as discussed in points (i) to (vi). These results, therefore, give an indication that occupation of low k-components of a high j orbit in the valence space and the role of np interaction in SOP orbits plays a crucial role in determining the overall deformation systematics of ^{224}Th to ^{234}Th isotopes.

3.2 *Yrast spectra*

In figure 1, the observed and calculated values of energies of various angular momentum states of $^{224-234}$Th isotopic mass chain are compared. The experimental level schemes of positive-parity yrast bands for $^{224-234}$Th are available up to spins 18^+, 20^+, 22^+, 24^+, 30^+ and 24^+ respectively. It is seen from figure 1, that the PSM calculation reproduces the available yrast energy levels up to known spins qualitatively. The maximum difference between theory and experiment for highest known spins is 0.220, 0.017, 0.025, 0.102, 0.119 and 0.172 (in MeV), respectively for $^{224-234}$Th. It is seen that the energy levels of these nuclei are reproduced well by the present calculation by taking the set of Nilsson parameters suggested by Rozmej [37] in the actinide region.

The present PSM calculations are performed by taking quadrupole–quadrupole plus monopole pairing plus quadrupole pairing Hamiltonian. In order to test whether the present calculation can reproduce the negative-parity bands without octupole deformation, the energies of these bands are obtained and compared with experimental data in figure 1. From this figure, it is seen that the PSM calculations reproduce the experimental transition energies for $^{228-234}$Th qualitatively, but shows disagreement for ^{224,226}Th. The

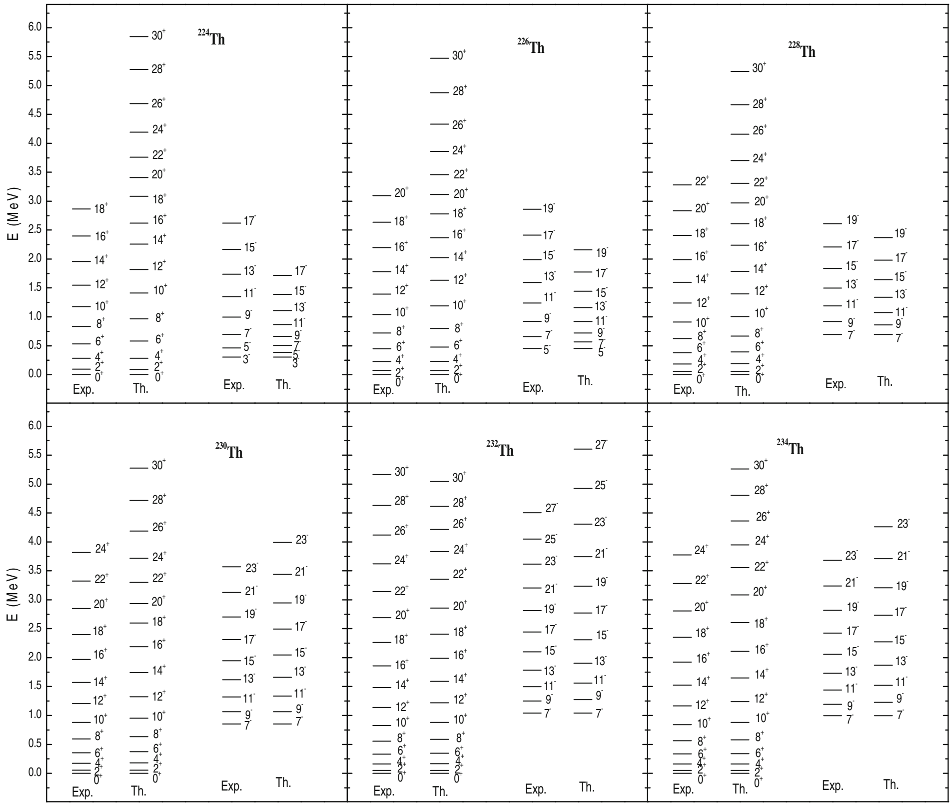

Figure 1. Comparison of calculated (Th.) and experimental (Exp.) positive and negative-parity bands of even–even $^{224-234}$Th isotopes. The experimental data are taken from refs [2–7].

relative positioning of the ground states of negative-parity bands with respect to 0^+ states of the corresponding positive-parity bands is not reproduced.

3.3 *Structure of Yrast states in thorium isotopes*

In figures 2a–f, the results of band diagrams for $^{224-234}$Th are presented. From these figures, it is observed that the yrast states in $^{224-234}$Th do not arise from a single intrinsic state. The yrast states up to a certain spin arise from a zero quasiparticle intrinsic state. After that spin, higher angular momentum states are found to arise from a different intrinsic state and may have a composite structure. They can arise from two or more intrinsic states. The details are described isotope-wise as follows:

Figure 2a represents the band diagram of ^{224}Th. This figure shows that the yrast states up to 14^+ arise from a zero quasiparticle state. After this spin, the zero quasiparticle band is crossed by two 2-qp neutron bands having $2\nu j_{15/2}[-3/2, 5/2]$, $K = 1$, $2\nu j_{15/2}[-3/2, -3/2]$, $K = 0$ configurations. The angular momentum states from 16^+ onwards arise from more than one intrinsic states and have a composite structure.

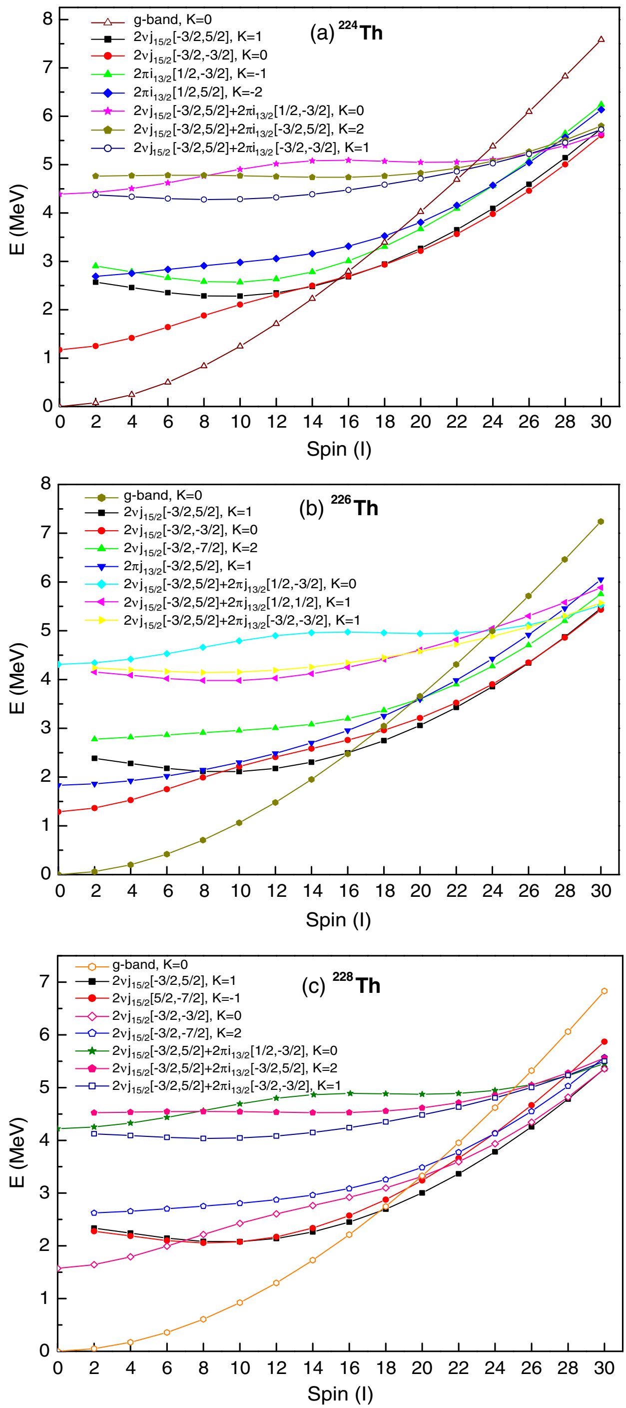

Figure 2. (**a–f**) Band diagrams (bands before configuration mixing) for $^{224-234}$Th. Only the important lowest lying bands in each configuration are shown.

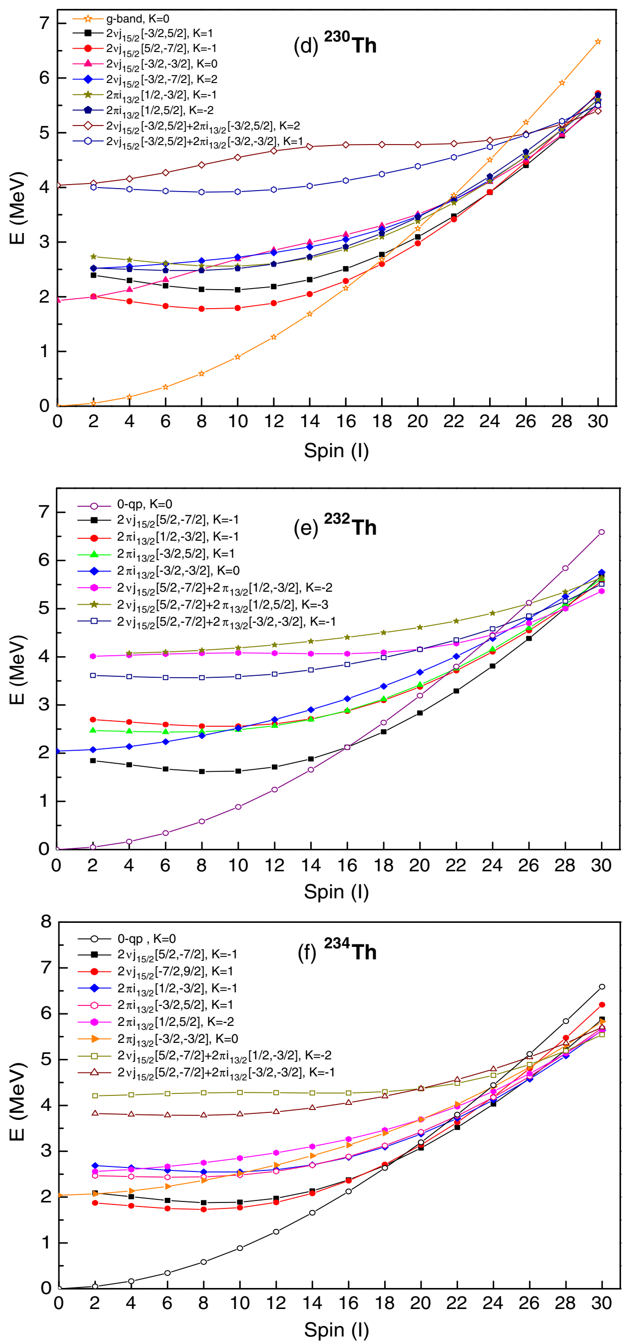

Figure 2. *Continued.*

Figure 2b represents the band diagram of ^{226}Th. It is evident from this figure that at 16^+ state the ground state band is crossed by a 2-qp neutron band having $2\nu \mathrm{j}_{15/2}[-3/2, 5/2]$, $K = 1$ configuration. It is noted that the yrast states up to 16^+ arise from a zero quasiparticle state. The yrast states 18^+ and 20^+ arise from the $2\nu \mathrm{j}_{15/2}[-3/2, 5/2]$, $K = 1$ band. The states with spin $I \geq 22^+$ have a composite structure arising from two 2-qp neutron bands having $2\nu \mathrm{j}_{15/2}[-3/2, 5/2]$, $K = 1$ and $2\nu \mathrm{j}_{15/2}[-3/2, -3/2]$, $K = 0$ configurations.

Figure 2c represents the band diagram of ^{228}Th. It is evident from this figure that between the spins 16^+ and 18^+, the ground-state band is crossed by a 2-qp neutron band having $2\nu \mathrm{j}_{15/2}[-3/2, 5/2]$, $K = 1$ configuration. It is noted that the yrast states up to 16^+ arise from a zero quasiparticle state. The yrast states 18^+–24^+ arise from $2\nu \mathrm{j}_{15/2}[-3/2, 5/2]$, $K = 1$ band. The state 26^+ onwards arises from more than one intrinsic states and have a composite structure.

Figure 2d represents the band diagram of ^{230}Th. It is evident from this figure that after spin 16^+ the ground state band is crossed by a 2-qp neutron band having $2\nu \mathrm{j}_{15/2}[5/2, -7/2]$, $K = -1$ configuration. It is noted that the yrast states up to 16^+ arise from a zero quasiparticle state. The yrast state 18^+ is arising from a 0-qp and a 2-qp neutron band whereas the yrast state 20^+ is arising from a 2-qp $2\nu \mathrm{j}_{15/2}[5/2, -7/2]$, $K = -1$ band. The states 22^+ and 24^+ arise from two 2-qp neutron bands having $2\nu \mathrm{j}_{15/2}[-3/2, 5/2]$, $K = 1$ and $2\nu \mathrm{j}_{15/2}[5/2, -7/2]$, $K = -1$ configurations. Thereafter, the yrast states are arising from more than two 2-qp bands.

Figure 2e represents the band diagram of ^{232}Th. It is evident from this figure that at 16^+ the ground-state band is crossed by a 2-qp neutron band having $2\nu \mathrm{j}_{15/2}[5/2, -7/2]$, $K = -1$ configuration. It is noted that the yrast states up to 16^+ arise from a zero quasiparticle state. The yrast states from 18^+ to 24^+ of this isotope arise from a 2-qp neutron band $2\nu \mathrm{j}_{15/2}[5/2, -7/2]$, $K = -1$ configuration. At spin 26^+ the two proton bands having $2\pi \mathrm{i}_{13/2}[1/2, -3/2]$, $K = -1$ and $2\pi \mathrm{i}_{13/2}[-3/2, 5/2]$, $K = 1$ configurations are also contributing to yrast spectra. The states with spin $\geq 28^+$ have a composite structure and in addition to the 2-qp proton and neutron bands, 4-qp bands are also contributing to the yrast states.

Figure 2f represents the band diagram of ^{234}Th. It is evident from this figure that at 18^+ state the ground-state band is crossed by two 2-qp neutron bands having $2\nu \mathrm{j}_{15/2}[5/2, -7/2]$, $K = -1$ and $2\nu \mathrm{j}_{15/2}[-7/2, 9/2]$, $K = 1$ configurations. It is noted that the yrast states up to 18^+ arise from a zero quasiparticle state. The yrast states 20^+ and 22^+ arise from two 2-qp neutron bands having $2\nu \mathrm{j}_{15/2}[5/2, -7/2]$, $K = -1$ and $2\nu \mathrm{j}_{15/2}[-7/2, 9/2]$, $K = 1$ configurations. In addition, there is contribution from two 2-qp proton bands having $2\pi \mathrm{i}_{13/2}[1/2, -3/2]$, $K = -1$ and $2\pi \mathrm{i}_{13/2}[-3/2, 5/2]$, $K = 1$ configurations. Above spin $I \geq 24^+$ the yrast states have a composite structure and are arising from more than two 2-qp and 4-qp bands.

3.4 *Electromagnetic quantities*

The reduced transition probabilities $B(EL)$ from the initial state (σ_i, I_i) to the final state (σ_f, I_f) are given by [24]

$$B(EL, I_\mathrm{i} \rightarrow I_\mathrm{f}) = \frac{e^2}{(2I_\mathrm{i} + 1)} |\langle \sigma_\mathrm{f}, I_\mathrm{f} \| \hat{Q}_\mathrm{L} \| \sigma_\mathrm{i}, I_\mathrm{i} \rangle|^2, \tag{8}$$

where $|\sigma,\ \mathrm{IM}\rangle$ is the wave function of eq. (1). Here, we are interested in $E2$ transitions from $I_{\mathrm{i}}^{+} = I$ to $I_{\mathrm{f}}^{+} = I-2$. Therefore, the operator Q_2 is related to the quadrupole operators by

$$Q_{2\nu} = e_{\nu}^{\mathrm{eff}}\sqrt{\frac{5}{16\pi}}\,Q_{\nu}^{2}$$

$$Q_{2\pi} = e_{\pi}^{\mathrm{eff}}\sqrt{\frac{5}{16\pi}}\,Q_{\pi}^{2}.$$

In the present calculation, we have used the effective charge for neutrons $e_{\nu}^{\mathrm{eff}} = 0.45e$ and for protons $e_{\pi}^{\mathrm{eff}} = 1.45e$.

The reduced matrix element appearing in eq. (8) is given by

$$\begin{aligned}
&\langle\sigma_{\mathrm{f}},\, I_{\mathrm{f}}\|\hat{Q}_{\mathrm{L}}\|\sigma_{\mathrm{i}},\, I_{\mathrm{i}}\rangle \\
&\quad = \sum_{\kappa_{\mathrm{i}},\kappa_{\mathrm{f}}} f_{\kappa_{\mathrm{i}}}^{\sigma_{\mathrm{i}}} f_{\kappa_{\mathrm{f}}}^{\sigma_{\mathrm{f}}} \sum_{M_{\mathrm{i}},M_{\mathrm{f}},M} (-)^{I_{\mathrm{f}}-M_{\mathrm{f}}} \begin{pmatrix} I_{\mathrm{f}} & L & I_{\mathrm{i}} \\ -M_{\mathrm{f}} & M & M_{\mathrm{i}} \end{pmatrix} \langle\phi_{\kappa_{\mathrm{f}}}|\hat{P}_{K_{\kappa_{\mathrm{f}}}M_{\mathrm{f}}}^{I_{\mathrm{f}}}\hat{Q}_{\mathrm{LM}}\hat{P}_{K_{\kappa_{\mathrm{i}}}M_{\mathrm{i}}}^{I_{\mathrm{i}}}|\phi_{\kappa_{\mathrm{i}}}\rangle \\
&\quad = 2\sum_{\kappa_{\mathrm{i}},\kappa_{\mathrm{f}}} f_{\kappa_{\mathrm{i}}}^{\sigma_{\mathrm{i}}} f_{\kappa_{\mathrm{f}}}^{\sigma_{\mathrm{f}}} \sum_{M',M''} (-)^{I_{\mathrm{f}}-K_{\kappa_{\mathrm{f}}}} (2I_{\mathrm{f}}+1)^{-1} \begin{pmatrix} I_{\mathrm{f}} & L & I_{\mathrm{i}} \\ -K_{\kappa_{\mathrm{f}}} & M' & M'' \end{pmatrix} \\
&\qquad \times \int \mathrm{d}\Omega\, D_{M''K_{\kappa_{\mathrm{i}}}}(\Omega)\langle\phi_{\kappa_{\mathrm{f}}}|\hat{Q}_{\mathrm{LM'}}\hat{R}(\Omega)|\phi_{\kappa_{\mathrm{i}}}\rangle.
\end{aligned} \tag{9}$$

The reduced transition probability $B(E2)$ values obtained from the PSM wave function for $^{224-234}$Th are presented in table 5. The $B(E2)$ values have been calculated by taking the same value of effective charge (i.e., 1.45 for protons and 0.45 for neutrons) for all the six $^{224-234}$Th isotopes. The experimental data for $B(E2)$ values of $^{224-228,234}$Th isotopes are available only for $2_1^+ \to 0_1^+$ transition [2,7,8]. The calculated $B(E2;\ 2_1^+ \to 0_1^+)$ values are in good agreement with experimental data for all the thorium isotopes except ^{224}Th. For ^{232}Th, the experimental $B(E2)$ values are known up to the transition from $26_1^+ \to 24_1^+$. From table 5, it is observed that the experimental $B(E2)$ values show an increasing trend up to spin 22^+. The calculated $B(E2)$ values are in good agreement with the experimental data and show an increase with spin up to 22^+. The experimentally observed dip at spin $I = 24^+$ is reproduced by the calculated results at the same spin. The experimental data of $B(E2)$ values of $^{224-230,234}$Th for higher spins are not available but we have predicted the theoretical values up to spin $I = 26^+$.

The gyromagnetic factors (g-factors) are defined by [24]

$$g(\sigma, I) = \frac{\mu(\sigma, I)}{\mu_N I} = g_{\pi}(\sigma, I) + g_{\nu}(\sigma, I), \tag{10}$$

with $g_{\tau}(\sigma, I)$, $\tau = \pi, \nu$ given by

$$\begin{aligned}
g_{\tau}(\sigma, I) = {} & \frac{1}{\mu_N[I(I+1)]^{1/2}}[g_l^{\tau}\langle\sigma, I\|\hat{J}^{\tau}\|\sigma, I\rangle \\
& + \left(g_s^{\tau} - g_l^{\tau}\right)\langle\sigma, I\|\hat{S}^{\tau}\|\sigma, I\rangle]
\end{aligned} \tag{11}$$

and $\mu(\sigma, I)$ is the magnetic moment of a state (σ, I).

Table 5. Comparison of calculated (Th.) and experimental (Exp.) $B(E2)$ reduced transition probabilities (in units of e^2b^2) for $^{224-234}$Th isotopes. Experimental data are taken from [2,5–8].

Transition	^{224}Th		^{226}Th		^{228}Th		^{230}Th		^{232}Th		^{234}Th	
($I_i^+ \rightarrow I_f^+$)	Exp.	Th.	Exp.	Th.	Exp.	Th.	Exp.	Th.	Exp.	Th.	Exp.	Th.
$2 \rightarrow 0$	0.80(06)	1.25	1.37(08)	1.42	1.41(05)	1.60	1.70(05)	1.77	1.74(07)	1.82	1.60(14)	1.90
$4 \rightarrow 2$	–	1.79	–	2.02	–	2.30	2.30(07)	2.54	2.51(21)	2.60	–	2.71
$6 \rightarrow 4$	–	2.00	–	2.27	–	2.55	–	2.81	2.86(19)	2.87	–	3.00
$8 \rightarrow 6$	–	2.12	–	2.40	–	2.69	–	2.96	3.02(13)	3.00	–	3.16
$10 \rightarrow 8$	–	2.21	–	2.50	–	2.79	–	3.06	3.19(18)	3.08	–	3.26
$12 \rightarrow 10$	–	2.28	–	2.58	–	2.87	–	3.13	3.25(26)	3.12	–	3.34
$14 \rightarrow 12$	–	2.33	–	2.60	–	2.94	–	3.18	3.42(26)	3.13	–	3.40
$16 \rightarrow 14$	–	0.17	–	1.66	–	2.88	–	3.12	3.42(35)	3.13		3.44
$18 \rightarrow 16$	–	2.42	–	1.98	–	0.70	–	2.73	3.95(61)	3.16		3.26
$20 \rightarrow 18$	–	2.58	–	2.51	–	2.69	–	2.97	3.16(53)	3.22		2.01
$22 \rightarrow 20$	–	2.62	–	2.57	–	2.81	–	3.13	3.68(96)	3.23		1.88
$24 \rightarrow 22$	–	2.66	–	2.62	–	2.86	–	3.17	2.11(61)	1.23		2.34
$26 \rightarrow 24$	–	2.72	–	2.67	–	2.91	–	3.20	3.07(05)	2.95		3.27

In our calculations, the following standard values of g_l and g_s are taken:

$$g_l^\pi = 1, \qquad g_l^\nu = 0,$$
$$g_s^\pi = 5.586 \times 0.75 \qquad \text{and} \qquad g_s^\nu = -3.826 \times 0.75,$$

where g_s^π and g_s^ν are damped by a usual 0.75 factor from the free-nucleon values to account for the core polarization and meson exchange current corrections [38–40]. We have used the same PSM wave function for the calculation of g-factors as used for $B(E2)$s.

In figures 3a and b, the results for Lande's g-factors for $^{224-234}$Th are presented. The theoretical values for the g-factors show a decrease at a certain spin in $^{224-230}$Th isotopes. Thereafter, the theoretical g-factors show an increasing trend. For example, in ^{224}Th

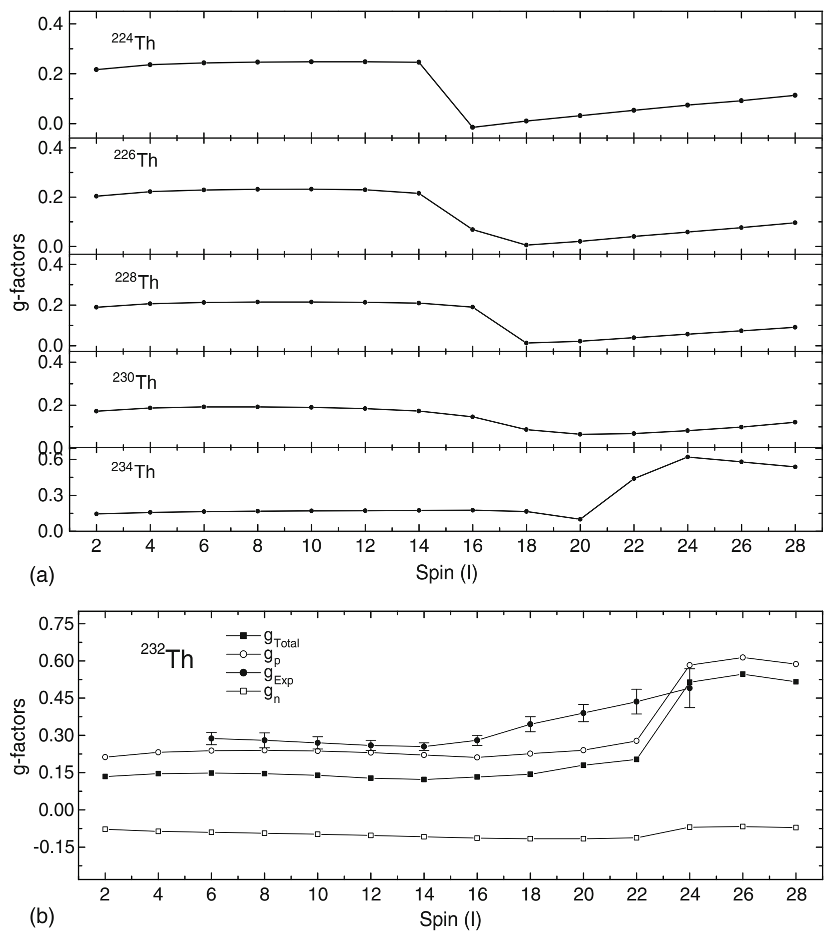

Figure 3. (**a**) Theoretical total g-factors as a function of angular momentum for $^{224-230,234}$Th. (**b**) Comparison of calculated g-factors with experimental data with the decomposition of total g-factor into proton and neutron contributions of ^{232}Th.

(figure 3a) the value of the theoretical g-factor is 0.246 at spin 14^+ whereas its value at 16^+ suddenly decreases to -0.014. Thereafter, the g-factor starts increasing with spin. The same trend is observed for g-factors of $^{226-230}$Th. These results can be understood by recalling band diagrams presented in figures 2a–e. For $^{224-230}$Th, the ground-state band is crossed by 2-qp neutron bands arising from the $1j_{15/2}$ orbit. Thus, the decrease in g-factors around the crossing region may be due to the alignment of neutrons in the $1j_{15/2}$ orbit. The experimental values of g-factors of $^{224-230,234}$Th are not known, and so we cannot make any comment but the present calculation predicts the neutron alignment in $^{224-230}$Th. In ^{232,234}Th, the g-factors show a reverse trend. In these isotopes, the g-factors at 20^+ are 0.094 and 0.100 whereas at 22^+ their values are 0.123 and 0.440, respectively, showing a sudden increase of g-factor. In ^{232}Th, the experimental values of g-factors for $I = 6^+$–24^+ states are known and there is experimental evidence that g-factors increase above spin $18\hbar$ and the increase of g-factors is attributed to the rotational alignment of $1i_{13/2}$ protons. The g-factors of $I \le 16\hbar$ are less than those for higher spins and thus gives evidence for the alignment of $1j_{15/2}$ neutrons. In figure 3b, the total g-factor and the contribution of the protons (g_p) and the neutrons (g_n) to the total g-factors are plotted as a function of spin (I). From this figure, it is seen that g_n is negative which shows decreasing trend up to spin $I = 16^+$ and g_p shows a decreasing trend up to spin 20^+. Thus, the negative values of g_n and decrease in g_p can be due to the alignment of neutrons. The total g-factor shows a small variation up to spin 14^+. Above spin 14^+ the total g-factor shows an increasing trend and a sudden increase is predicted around spin 24^+. The sudden increase in g_p is also observed. Thus, at higher spin the total g-factor is mainly due to g_p contribution and that may be due to the alignment of protons. From the analysis of the band diagram of ^{232}Th (figure 2e), it is seen that the first crossing is due to 2-qp neutron band from the $1j_{15/2}$ orbit and second crossing is around spin 24^+ which is due to the crossing of 2-qp proton bands from the $1i_{13/2}$ orbit. Thus, the present calculation predicts neutron alignment below first crossing and proton alignment around the second crossing that is consistent with the experimental data. However, the present calculation shows a sharp increase in the g-factor at spin 24^+. The CHFB [14] calculation predicted only neutron alignment in ^{232}Th. In the present calculation both neutron and proton alignments are seen and these are due to the alignment of a pair of neutrons in $1j_{15/2}$ orbit and protons in $1i_{13/2}$ orbit. The sudden changes occurring in g-factors (increase or decrease) at a certain spin clearly indicate that the yrast spectra of the nuclei should undergo a structural change at that spin.

4. Conclusions

From the PSM study of $^{224-234}$Th, the following broad conclusions can be drawn:

(i) The results on band diagrams show that the yrast spectra in Th isotopes for spin less than 16^+ arise from a single 0-qp intrinsic state. As one goes to higher angular momentum states, it is observed that the intrinsic state changes and has multi-qp configuration. Some of the angular momentum states are found to have composite structure, that is, they arise from more than one intrinsic state.

(ii) The results presented on the $B(E2; 2_1^+ \rightarrow 0_1^+)$ transition probability are found to show reasonably good agreement with the available experimental data for all the isotopes. In ^{232}Th, the observed dip in the $B(E2)$ values at $I = 22^+$ is reproduced by the PSM calculations.

(iii) The theoretical results for Lande's g_I factors show a decrease at a certain spin in $^{224-230}$Th isotopes, thereafter the theoretical g_I factors show an increasing trend. This needs to be experimentally tested. In ^{232,234}Th, g_I are found to show a reverse trend, that is, they show a sudden increase of g_I factors. The experimentally observed values of g_I factors for ^{232}Th are found to be in agreement with theoretical values qualitatively. In addition, the present calculation reproduces the proton and neutron alignments observed experimentally in ^{232}Th.

Acknowledgements

The authors are grateful to Prof. Y Sun and Prof. J A Sheikh for their collaborations and most valuable discussions. One of the authors (DR) is grateful to UGC, New Delhi, India, for providing financial assistance under RGNJRF.

References

[1] I Y Lee, *Nucl. Phys. A* **520**, 641c (1990)
[2] A A Cohen, *Nucl. Data Sheets* **80**, 227 (1997)
[3] Y A Akovali, *Nucl. Data Sheets* **77**, 433 (1996)
[4] N Azmal *et al*, *J. Phys.: G Nucl. Part. Phys.* **25**, 831 (1999)
[5] E Browne and J K Tuli, *Nucl. Data Sheets* **113**, 2113 (2012)
[6] E Browne, *Nucl. Data Sheets* **107**, 2579 (2006)
[7] E Browne and J K Tuli, *Nucl. Data Sheets* **108**, 681 (2007)
[8] S Raman, C W Nestor Jr and P Tikkanen, *At. Data Nucl. Data Tables* **78**, 82 (2001)
[9] S Raman, C H Malarkey, W T Milner, C W Nestor Jr and P H Stelson, *At. Data Nucl. Data Tables* **36**, 1 (1987)
[10] O Hausser *et al*, *Phys. Rev. Lett.* **48**, 383 (1982)
[11] J F C Cocks *et al*, *Nucl. Phys. A* **645**, 61 (1999)
[12] N V Zamfir and D Kusnezov, *Phys. Rev. C* **63**, 054306 (2001)
[13] S M Diab, *Prog. Phys.* **2**, 97 (2008)
[14] M Diebel and U Mosel, *Z. Phys. A* **303**, 131 (1981)
[15] W Nazarewicz and P Olanders, *Nucl. Phys. A* **441**, 420 (1985)
[16] J L Egido and P Ring, *Nucl. Phys. A* **423**, 93 (1984)
[17] K Hara and Y Sun, *Int. J. Mod. Phys. E* **4**, 637 (1995)
[18] Y Sun and D H Feng, *Phys. Rep.* **264**, 375 (1996)
[19] B D Sehgal, R Devi and S K Khosa, *J. Phys. G* **32**, 1211 (2006)
[20] B A Bian, Y M Di, G L Long, Y Sun, J Zhang and J A Sheikh, *Phys. Rev. C* **75**, 014312 (2007)
[21] Y C Yang, Y Sun, S J Zhu, M Guidry and C L Wu, *J. Phys. G* **37**, 085110 (2010)
[22] S Verma, R Devi and S K Khosa, *Eur. Phys. J. A* **30**, 531 (2006)
[23] S G Nilsson, C F Tsang, A Sobiczewski, Z Szymanski, S Wycech, C Gustafson, I L Lamm, P Moller and B Nilsson, *Nucl. Phys. A* **131**, 1 (1969)
[24] Y Sun and J L Egido, *Nucl. Phys. A* **580**, 1 (1994)
[25] L Grodzins, *Phys. Lett.* **2**, 88 (1962)
[26] R F Casten *et al*, *Phys. Lett.* **47**, 1433 (1981)
[27] P Federman and S Pittel, *Phys. Lett. B* **69**, 385 (1977)

[28] S C K Nair, A Ansari and L Satpathy, *Phys. Lett. B* **71**, 257 (1977)
[29] S Pittel, *Nucl. Phys. A* **347**, 417 (1980)
[30] M Danos and V Gillet, *Phys. Rev.* **161**, 1034 (1967)
[31] A Arima and V Gillet, *Ann. Phys. (N.Y.)* **66**, 117 (1971)
[32] A Arima, T Otsuka, F Iachello and I Talmi, *Phys. Lett. B* **66**, 205 (1977)
[33] P Federman, S Pittel and R Compos, *Phys. Lett. B* **35**, 9 (1979)
[34] P Federman and S Pittel, *Phys. Lett. B* **77**, 29 (1978)
[35] P Federman and S Pittel, *Phys. Rev. C* **20**, 820 (1979)
[36] P K Mattu and S K Khosa, *Phys. Rev. C* **39**, 2018 (1989)
[37] P Rozmej, GSI-Preprint 85–41 (1985)
[38] A Bohr and B R Mottelson, *Nuclear structure* (W A Benjamin, New York, Amsterdam, 1969) Vol. I
[39] B Castel and I S Towner, *Modern theories of nuclear moments* (Clarendon Press, Oxford-Clarendon, 1990)
[40] J Rikovska *et al*, *Phys. Rev. Lett.* **85**, 1392 (2000)